

# Direction-Selective Dendritic Action Potentials in Rabbit Retina

Nicholas Oesch,<sup>1</sup> Thomas Euler,<sup>2</sup>  
and W. Rowland Taylor<sup>1,\*</sup>

<sup>1</sup>Neurological Sciences Institute  
Oregon Health and Sciences University  
Beaverton, Oregon 97006

<sup>2</sup>Max-Planck-Institute for Medical Research  
D-69120 Heidelberg  
Germany

## Summary

Dendritic spikes that propagate toward the soma are well documented, but their physiological role remains uncertain. Our *in vitro* patch-clamp recordings and two-photon calcium imaging show that direction-selective retinal ganglion cells (DSGCs) utilize ortho-grade dendritic spikes during physiological activity. DSGCs signal the direction of image motion. Excitatory subthreshold postsynaptic potentials are observed in DSGCs for motion in all directions and provide a weakly tuned directional signal. However, spikes are generated over only a narrow range of motion angles, indicating that spike generation greatly enhances directional tuning. Our results indicate that spikes are initiated at multiple sites within the dendritic arbors of DSGCs and that each dendritic spike initiates a somatic spike. We propose that dendritic spike failure, produced by local inhibitory inputs, might be a critical factor that enhances directional tuning of somatic spikes.

## Introduction

More than 40 years ago, electrophysiological recordings documented the presence of fast prepotentials in hippocampal neurons (Spencer and Kandel, 1961). Subsequent work suggested that such events represent spikes initiated within the dendrites and that these spikes propagate to the soma and initiate action potentials at the soma or initial axonal segment (Llinas and Nicholson, 1971; Schwindt and Crill, 1997; Spencer and Kandel, 1961; Turner et al., 1991). Direct dendritic recordings have corroborated and extended these findings using electrophysiological (Chen et al., 1997; Golding and Spruston, 1998; Hausser et al., 2000; Martina et al., 2000; Schwindt and Crill, 1997; Stuart et al., 1997; Velte and Masland, 1999) and optical techniques (Djurišić et al., 2004; Kasuga et al., 1993). It is evident that the site of action potential initiation can depend on the characteristics of the stimulus driving the neuron (Chen et al., 1997; Martina et al., 2000). Moreover, dendritic spikes initiated within functionally isolated dendritic compartments can propagate to the soma even in the

presence of continuous synaptic activity (Williams, 2004). Direct dendritic recordings have also shown that action potentials initiated in the soma can backpropagate into the dendrites of several types of neurons (Spruston et al., 1995; Stuart et al., 1997; Stuart and Sakmann, 1994). The extent to which dendritic action potentials contribute to neural computation remains unresolved.

Fohlmeister and Miller (1997) predicted from their modeling studies that the dendrites of retinal ganglion cells are active. Dendritic spikes have been observed in  $\alpha$ -ganglion cells, which have large somas and thick primary dendrites (Velte and Masland, 1999). In that study, spikes were elicited by current injection into either the soma or dendrite, and therefore it is not known whether dendritic spikes are generated during light-evoked activity. In this study, we provide evidence for light-evoked dendritic spikes in a well-defined class of retinal ganglion cell, the direction-selective ganglion cell (DSGC) (Taylor and Vaney, 2003; Vaney and Taylor, 2002).

DSGCs, which make up about 10% of the ganglion cells in the rabbit retina (Vaney, 1994), signal the direction of image motion across their receptive fields by firing action potentials in a preferred direction, and not in the opposite, or null, direction. These cells are ON/OFF ganglion cells, meaning that the cell responds to the onset and termination of a light flash. The ON and OFF postsynaptic potentials (PSPs), which comprise excitatory and inhibitory components (Taylor and Vaney, 2002), are received through two separate dendritic arbors that stratify narrowly at distinct levels within the inner plexiform layer. The extents of these two dendritic arbors define the extent of the receptive fields for ON and OFF responses (Yang and Masland, 1992). The outer, or OFF dendritic arbor is furthest from the soma and responds only to light decrements, while the inner, or ON dendritic arbor responds to light increments. A practical consequence of the dendritic structure is that the experimenter can selectively stimulate only one dendritic arbor by the choice of stimulus contrast. For example, the leading edge of a dark stimulus bar moving across the receptive field will activate the OFF dendritic arbor, while the trailing edge of the same stimulus bar will activate the ON dendritic arbor. Because the axon arises from the soma in these cells, signals must pass through the soma before reaching the axon.

Under some conditions we observed small spike-like events elicited in response to physiological stimulation of DSGCs, and therefore we postulated that these events might represent dendritic spikes. In this paper, we investigate the properties of these putative dendritic spikes and show that spike generation allows transmission of salient sensory inputs and precludes the transmission of information during inappropriate stimuli. We propose that dendritic spikes have a clear physiological role in dramatically increasing the directional tuning of these cells.

\*Correspondence: taylorw@ohsu.edu

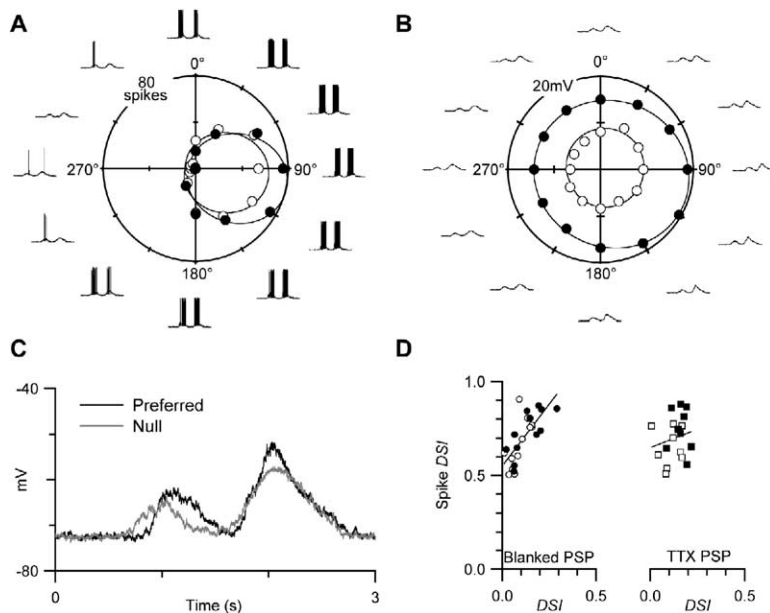


**Figure 1. Spike Generation Sharpens Directional Tuning**

(A) Current-clamp recordings are shown adjacent to the stimulus angle. Spikes are observed during the leading and trailing edge of the stimulus. Since the stimulus was a bright bar, the leading edge response activated the ON dendritic arbor (solid symbols), while the trailing edge activated the OFF arbor (open symbols). Each point on the polar plot shows the total number of spikes elicited during each response. The ON and OFF responses have essentially the same preferred direction. The continuous line shows best-fit von Mises distribution for the ON and OFF responses. The preferred directions obtained from the fits were 97° and 103° for the ON and OFF responses, respectively. The DSI values for the ON and OFF responses were 0.5 and 0.63, respectively.

(B) TTX (0.5  $\mu$ M) was added to the bath solution to block spiking. The continuous line shows best-fit von Mises distributions for the ON and OFF responses. The preferred directions obtained from the fits were 83° and 110° for the ON and OFF responses, respectively.

spectively. The DSI values for the ON and OFF responses were 0.04 and 0.21, respectively.

(C) Current-clamp responses from the same cell to preferred (black line) and null direction motion (gray line). The first PSP represents the leading edge, ON response, and the second PSP represents the trailing edge, OFF response.

(D) DSIs measured from spike counts plotted against DSIs measured from PSP amplitudes in 12 cells (open symbols = ON responses; closed symbols = OFF responses). Left panel (circles) shows the DSIs of the PSPs determined by blanking the spikes, as described in the [Experimental Procedures](#). The regression coefficient for the best-fit line was 1.31 ( $r^2 = 0.53$ ). In 9 of the 12 cells (right panel, squares), PSP DSIs were measured during bath application of TTX. The regression coefficient for the best-fit line was 0.39 ( $r^2 = 0.04$ ).

## Results

### Action Potentials Sharpen Directional Tuning in DSGCs

The strength of the directional tuning can be quantified using a directional tuning index (DSI) (see [Experimental Procedures](#)) that ranges between zero and one, with larger values being more directional. The DSI measured from spikes in current-clamp recordings averaged  $0.67 \pm 0.13$  for the ON response and  $0.74 \pm 0.13$  for the OFF response, similar to DSIs of  $0.53 \pm 0.13$  and  $0.64 \pm 0.12$  obtained from extracellular spike recordings in the same 12 cells ([Figure 1A](#)). The angle of the preferred direction did not differ between current-clamp and extracellular recording conditions ( $p > 0.6$ , paired Student's *t* test). The DSI was also estimated from the PSP amplitude under current-clamp conditions. In order to measure the PSP amplitude, we removed spikes either digitally during offline analysis or pharmacologically by adding 0.5  $\mu$ M TTX to the superfusion solution ([Figure 1B](#)). The directional difference in the amplitude of PSPs varied widely in the group of cells. In the same group of cells used to estimate DSI from spikes, DSI measured from spike-blanked PSPs was  $0.09 \pm 0.05$  for the ON response and  $0.14 \pm 0.08$  for the OFF response ( $n = 12$ ). When TTX was applied, DSI was  $0.11 \pm 0.05$  for the ON response and  $0.16 \pm 0.04$  for the OFF response ( $n = 10$ ). These low DSI values corresponded to PSP amplitude differences between preferred and null direction stimuli that ranged from 0 to 7.8 mV with a mean of  $3.7 \pm 1.7$  mV for the ON response, and  $-3.7$  to 10.1 mV with a mean of  $3.8 \pm 3.0$  mV for the OFF response ([Figure 1C](#)).

The spike DSI displayed a weak positive correlation with the PSP DSI measured from blanked PSPs (regression coefficient of the best fit line was 1.3;  $r^2 = 0.53$ ); however, the spike DSI was not dependent on PSP DSI recorded during bath application of TTX (regression coefficient was 0.39;  $r^2 = 0.04$ ; [Figure 1D](#)). The reason for the weak correlation is unclear but may relate to the presence of voltage-gated sodium channels in the dendrites. On average, the DSI observed for spikes was about 6-fold higher than the PSP DSI. The enhanced directional tuning is also evident from the close correlation in the preferred directions for the ON and OFF responses. The difference in the preferred directions between the ON spikes and OFF spikes was  $12^\circ \pm 9^\circ$ , while this difference for PSPs was  $38^\circ \pm 52^\circ$  ( $n = 12$ ). These results indicate that spike initiation is a potent mechanism for sharpening directional tuning in these cells.

### Spike Initiation Does Not Occur at the Soma for Light-Evoked Spikes

Dark-adapted DSGCs had a resting potential of  $-70.7 \pm 1.6$  mV ( $n = 13$ ) and an input resistance of  $82.0 \pm 20.6$  M $\Omega$  ( $n = 9$ ). They displayed little spontaneous synaptic input and had no background spiking. Depolarizing current steps elicited sustained trains of action potentials that displayed prominent afterhyperpolarizations. During hyperpolarizing steps, an early transient component was observed, suggesting the presence of  $I_h$  currents in the DSGCs ([Figure 2A](#)). Above threshold, spike frequency was a linear function of injected current, with a slope of  $0.31 \pm 0.18$  Hz/pA ( $n = 9$ ; [Figure 2C](#)).

Light stimuli were more potent than direct somatic

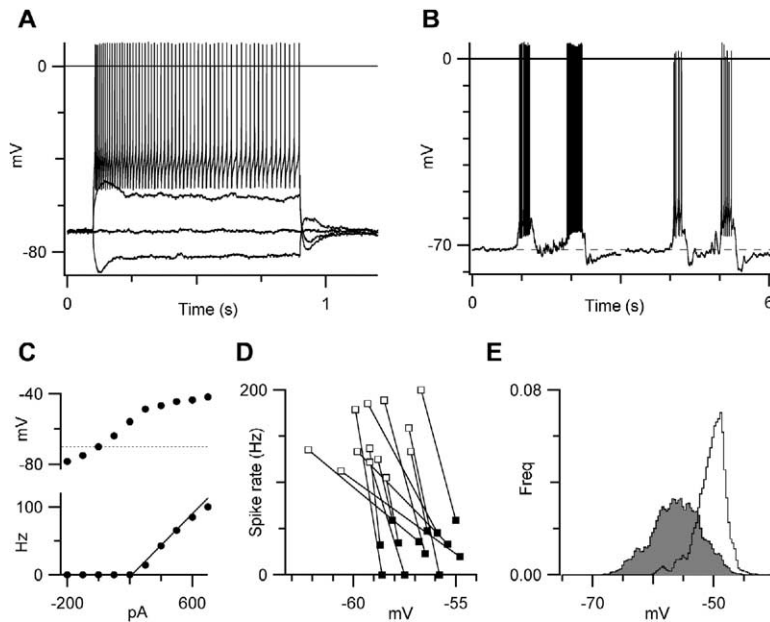


Figure 2. Light Stimuli Are More Potent at Generating Spikes Than Direct Current Injection

(A) Current-clamp recordings showing responses to  $-100$ ,  $0$ ,  $100$ , and  $200$  pA current steps.

(B) Response to a bright bar moving in the preferred direction (left trace) and a response from the same cell to direct current injection of a PSP waveform into the soma (right trace). The PSP waveform for the injected current was taken from a previously recorded light response in the same cell. In this example, the light stimulus generated  $130$  spikes/s, while the current-injected response produced  $36$  spikes/s.

(C) The upper panel shows the average membrane potential reached during  $800$  ms depolarizing current pulses. The dotted line shows the resting membrane potential. The lower panel shows the mean spike rate during depolarizing pulses. Above spike threshold, injected current generated  $0.28$  Hz/pA. The average for nine cells was  $0.31 \pm 0.18$  Hz/pA.

(D) Spike rate versus mean depolarization

level. Light stimuli (open circles) produced higher spike rates at similar or less depolarized levels than responses to direct current injection, which mimicked the light-evoked PSPs in the same cells.

(E) Light-evoked spikes and current injection-evoked spikes were generated as described in (B). Spike threshold measurements from ten cells were combined to produce probability density distributions for light-evoked spike thresholds (shaded histogram) and depolarization-evoked spike thresholds (open histogram).

depolarization for generating spikes in DSGCs (Figures 2B, 2D, and 2E). The peak of light-evoked PSPs reached  $-59.1 \pm 1.5$  mV, or  $11.6 \pm 1.5$  mV depolarized from the resting potential, and generated  $59 \pm 21$  spikes/stimulus. The mode of the interspike interval (ISI) distribution corresponded to a spike rate of  $148 \pm 30$  Hz (Figure 2D, open squares;  $n = 13$  cells). In each cell, we also injected current through the recording electrode with a waveform generated from PSPs recorded in response to light stimuli for that cell (Figure 2B; see Experimental Procedures). Using this PSP current command waveform, we generated a series of somatic PSPs that bracketed the amplitude of the light-evoked PSP. Invariably, one of these current-injected PSPs would closely match the light-evoked PSP in both amplitude and shape. Injected current waveforms that depolarized the soma to equivalent or slightly more depolarized potentials as the light-evoked PSPs produced  $11 \pm 9$  spikes/stimulus at a modal ISI corresponding to a spike rate of  $41 \pm 47$  Hz (Figure 2D, closed squares). The average peak depolarization reached  $-56.8 \pm 1.3$  mV, or  $13.9$  mV depolarized from the resting potential. This value is  $2.3$  mV more depolarized than the peak depolarization for the light-evoked PSPs in the same cells, yet it produced a significantly lower spike rate and absolute number of spikes ( $p < 0.001$ , paired Student's *t* test).

These results suggest that the membrane potential at the soma is a poor predictor of spike initiation during light-evoked PSPs. Direct analysis of the spike threshold confirms this expectation. The spike threshold (see Experimental Procedures) was measured during current-injected and light-evoked PSPs in ten cells. In order to obtain a comparable number of spikes under the two conditions, current-injected PSPs that reached

more depolarized mean potentials were also analyzed. The probability density distribution of light-evoked spike thresholds was symmetric with a broad monotonic peak at  $-56$  mV, and a width at half height of  $\sim 8$  mV ( $2117$  spikes; Figure 2E). The peak was approximately centered on the mean PSP amplitude, suggesting that spikes are most likely to occur during a PSP, but the broadness and symmetry of the distribution indicate that spike initiation is essentially uncorrelated with membrane potential during the PSP. The probability density distribution for spike thresholds during current-injected PSPs displayed a narrower peak at  $-49$  mV, and a width at half height of  $\sim 4$  mV ( $1233$  spikes; Figure 2E). The distribution was skewed, with a tail toward negative potentials that arose because spike threshold was initially low and in some cells increased during the current-injected PSPs. The increase in threshold presumably resulted from sodium channel inactivation during the depolarization. The results indicate that somatic spike threshold, probed with depolarizing current injection, is considerably more depolarized than the mean light-evoked PSP amplitude, demonstrating that the PSP amplitude at the soma is not the critical factor for generating directional spike discharge. Therefore, we considered the possibility that spike initiation might occur in the dendrites.

#### Spike Initiation Occurs in the Dendrites

Previous work has shown that it is possible to reveal the presence of active dendritic responses when somatic spiking is suppressed by local application of TTX to the soma (Huguenard et al., 1998; Regehr et al., 1993; Turner et al., 1989, 1991). To investigate the active properties of the dendrites, preferred direction stimuli were presented to a cell every 16 s, while a pipette filled

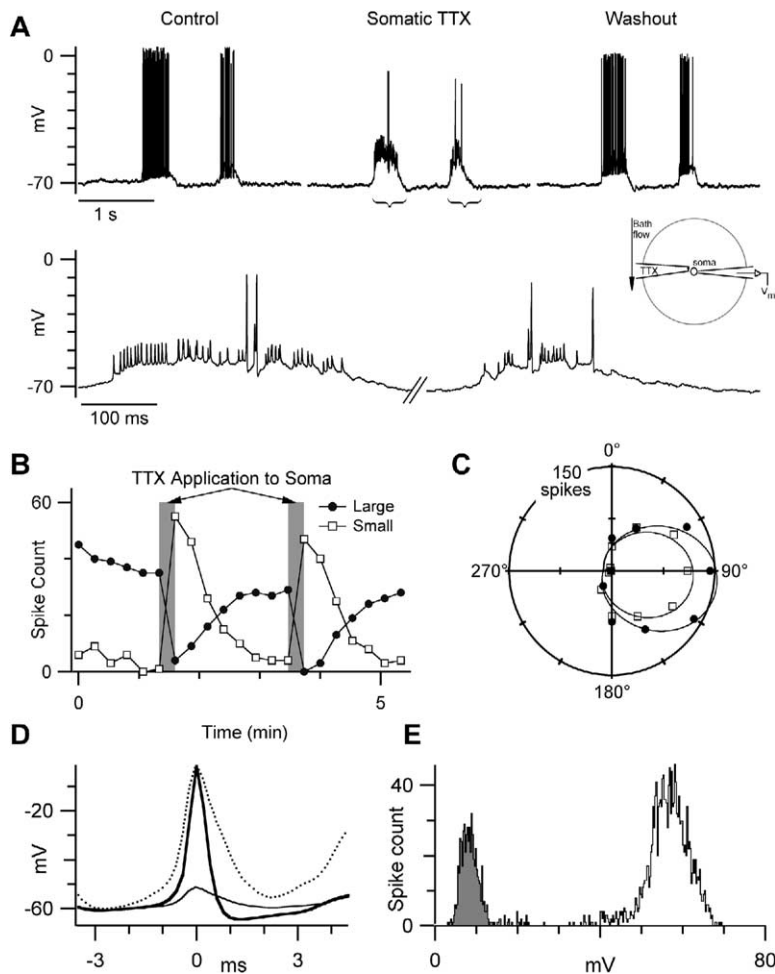


**Figure 3. Local TTX Application to the Soma Reveals Dendritic Spikes**

(A) Current-clamp responses to a dark bar moving in the preferred direction before, during, and after local application of 1  $\mu$ M TTX to the soma. The lower panel shows, on an expanded time axis, sections of the upper middle trace denoted by brackets. The inset schematic shows the positions of the TTX and recording electrodes in relation to the soma and the dendritic arbor (outer circle).

(B) Total spike counts for ON and OFF responses during preferred direction stimuli presented every 16 s. Gray regions indicate periods of 1  $\mu$ M TTX application to the soma.

(C) Polar plot of the total spike count for somatic spikes during a control period (open squares) and dendritic spikes during a period of 1  $\mu$ M local TTX application (solid circles). The solid lines show the best-fit von Mises distributions, with preferred directions of 96° and 98° for the control and TTX data and DSI values of 0.56 and 0.62.

(D) The thick trace shows the average of 679 somatic spikes, and the thin trace shows the average of 515 dendritic spikes from one cell. The broken line shows the dendritic spike scaled to match the somatic spike amplitude. Spikes were averaged by aligning the peaks at time zero.

(E) Amplitude distribution histograms of 1726 somatic spikes (black) and 582 dendritic spikes (gray) derived from preferred direction stimuli before, during, and upon washout of local TTX application to the soma. Twelve other cells displayed similar results.

with extracellular solution containing 1  $\mu$ M TTX was moved to within about 10  $\mu$ m of the cell soma. Positive pressure was applied to the pipette to eject the TTX solution onto the soma. During somatic TTX application, action potentials were suppressed and replaced by smaller fast potentials (Figure 3A). The effect of TTX was rapid and reversible (Figure 3B). The directional tuning of the small spikes was identical to that of the large spikes (Figure 3C). The large spikes were brief and displayed an afterhyperpolarization, whereas the small spikes were broader and lacked the afterhyperpolarization (Figure 3D). The large and small spikes are clearly separated in amplitude histograms (Figure 3E). In all cells, the spike amplitudes showed a strong bimodal distribution, with one peak at  $7.4 \pm 1.9$  mV representing the small spikes and a second peak at  $54.8 \pm 3.5$  mV representing the large spikes. It is important to note that inclusion of TTX in the bath solution completely eliminated both large and small spikes (Figures 1B and 1C), indicating that TTX-sensitive sodium channels in the dendrites mediate the putative dendritic spikes.

If the large spikes are somatic and the small spikes are dendritic, then it should also be possible to block somatic spikes and reveal dendritic spikes using the intracellular sodium channel blocker QX-314, a lido-

caine derivative (Pinato and Midgaard, 2005). In order to obtain sufficient control responses, the tip of the patch electrode was filled with drug-free solution, and the electrode was backfilled with intracellular solution containing 1–10 mM QX-314. At the higher concentrations, all spike activity was quickly suppressed. At concentrations of 1–2 mM, somatic spikes were suppressed, revealing the presence of smaller dendritic spikes (see the Supplemental Data available with this article online). Similar to bath application of TTX, spiking was completely suppressed in five of the seven cells. In two cells, the recording was lost before complete suppression could be observed. We will provide further evidence supporting our hypothesis that the small spikes are initiated in the dendrites and propagate to the soma, where they initiate the larger spikes. In the following, we will refer to the small and large spikes as dendritic and somatic, respectively.

If dendritic spikes can be independently initiated in separate dendritic branches, then spikes from separate dendrites should not be refractory to each other and should be able to superimpose (Larkum et al., 2001). In contrast, somatic spikes should display an absolute refractory period. These expectations are borne out by analysis of the ISI distributions during experiments similar to that shown in Figure 3. Responses included con-

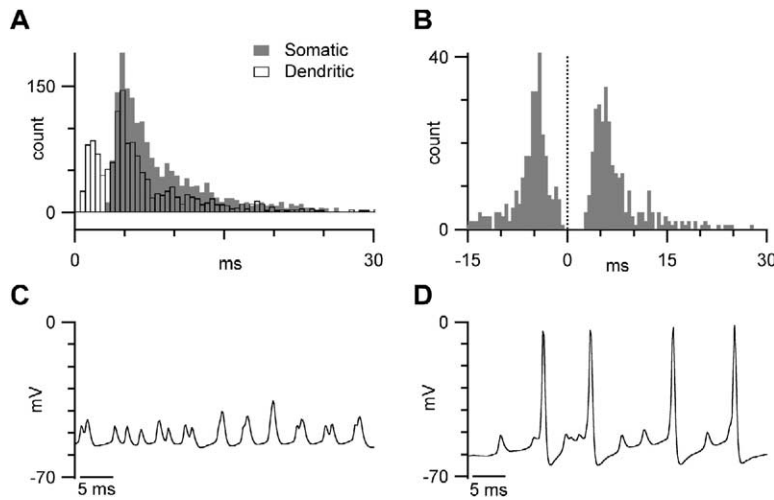


Figure 4. Interspike Interval Analysis Shows that Many Dendritic Spikes Are Not Refractory

TTX was applied locally to the soma to reveal dendritic spikes during preferred direction stimuli. (A) Interspike interval distributions for somatic spikes under control conditions (gray bars) and dendritic spikes during local TTX application (open bars). (B) Analysis of interspike intervals between somatic and dendritic spikes. During onset or washout of somatic TTX application, responses often displayed a mixture of large and small spikes. The histograms show the timing of dendritic spikes relative to the somatic spikes that occurred at time zero. Negative interspike intervals indicate dendritic spikes that precede the somatic spike; positive intervals represent dendritic spikes that follow the somatic spike. (C) An expanded section of a light response during local 1  $\mu$ M TTX application showing superposition of dendritic spikes. (D) An expanded section of a light response during local 1  $\mu$ M TTX application showing a mixture of large and small spikes.

control periods, where no dendritic spikes were seen, and periods of local somatic TTX application, where a mixture of somatic and dendritic spikes was seen. The somatic spikes displayed an absolute refractory period of  $3.5 \pm 0.7$  ms ( $n = 9$ ; gray bars in Figure 4A). Analysis of dendritic spikes revealed a shorter refractory period (open bars in Figure 4A). The decline in the dendritic ISI histogram near zero is due to a limit on the shortest resolvable ISI (see Experimental Procedures). Examination of the raw responses (Figures 4C and 4D) shows superposition of the dendritic spikes, indicating that many dendritic spikes were not refractory. Results that were similar to those in Figure 4 were obtained in all nine cells analyzed.

If spikes are initiated in the dendrites and propagate to the soma, then it might be possible for somatic spikes to backpropagate into the dendrites. Moreover, a backpropagating somatic spike might render the dendrites refractory. We were able to confirm this prediction by analyzing the timing of dendritic spikes that preceded or followed a somatic spike in records where a mixture of events was seen. Dendritic spikes did not appear within the refractory period following a somatic spike (Figure 4B); however, examination of the records shows directly that dendritic spikes can occur at any time before a somatic spike (Figures 4B and 4D). Backpropagation of somatic spikes might explain why in some cells there were more dendritic spikes per stimulus during local TTX application than somatic spikes in control (Figure 3B). Multiple spike initiation sites could generate dendritic spikes in different dendrites; however, the first dendritic spike to reach the soma will elicit a somatic spike, which will backpropagate and cancel any coincident dendritic spikes.

If dendritic spikes initiate somatic spikes, then injecting hyperpolarizing current into the soma should reduce the efficacy of somatic spike initiation and reveal the underlying dendritic spikes. Indeed, progressively larger hyperpolarizing current steps reduced the num-

ber of somatic spikes with a concomitant increase in the number of dendritic spikes (Figures 5A and 5B). Similar to dendritic spikes observed during local TTX application, the small spikes revealed during hyperpolarizing pulses could be clearly distinguished from the somatic spikes based on amplitude (Figure 5C). Overall, there was a tendency to observe more ON than OFF dendritic spikes. In some cells, we observed dendritic spikes only during ON responses, and not during OFF responses (data not shown). The observation that the spiking properties of the DSGCs are dependent on the contrast of the light stimulus, and thus the dendritic origin of the signals, provides further evidence for multiple spike initiation zones in the dendrites.

If light-evoked spikes are first initiated in the dendrites, then we should be able to block light-evoked somatic spikes by applying TTX to the dendrites (Huguenard et al., 1998; Regehr et al., 1993; Turner et al., 1989, 1991). We tested this prediction by placing a pipette containing TTX in the inner plexiform layer, 10–20  $\mu$ m beneath the inner limiting membrane of the retina, and approximately 80–200  $\mu$ m from the cell soma. We applied 30–60 s pulses of 0.5  $\mu$ M TTX to the dendrites. To monitor the excitability of the soma, a depolarizing current pulse followed each preferred direction stimulus. In all eight cells, we were able to observe a selective reduction from 13% to 73% (average  $41.5\% \pm 15\%$ ) in the number of light-evoked spikes (Figures 6A and 6B). In every case, there was a smaller concomitant reduction ( $25.2\% \pm 7.8\%$ ) in the depolarization-activated spikes, which we attribute to the spread of TTX. However, it is important to emphasize the qualitative difference between somatic and dendritic TTX application. In contrast to somatic TTX application, dendritic TTX application, which selectively reduced light-evoked spiking, did not promote the unmasking of dendritic spikes; it simply reduced the number of spikes (Figure 6A). These results are consistent with the hypothesis that orthograde dendritic spikes initiate somatic spikes.

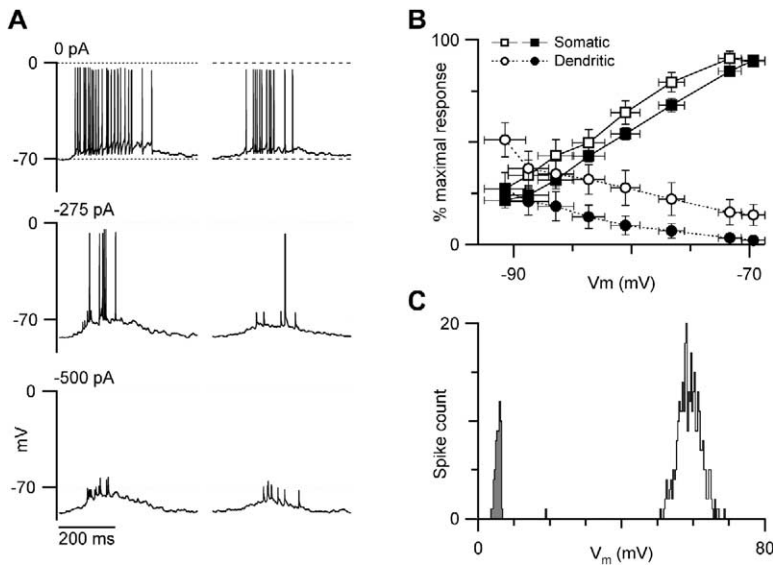


**Figure 5. Hyperpolarizing the Soma Unmasks Dendritic Spikes**

(A) Evoked responses from preferred direction motion during hyperpolarizing current injection. The left traces are OFF responses, and the right traces are ON responses.

(B) Preferred direction stimuli were presented during current pulses between +25 and -500 pA. The x axis shows the average baseline potential during the current step. The y axis shows the percentage of somatic ON and OFF spikes and dendritic ON and OFF spikes relative to the number of somatic spikes recorded at the resting potential (solid and open symbols are OFF and ON responses, respectively; square and round symbols are somatic and dendritic spikes, respectively). Each point represents the averaged data from ten cells. The error bars show standard deviations.

(C) Amplitude histograms of the spikes elicited by preferred direction stimuli presented during current pulses that hyperpolarized the cell over the potential range shown in (B). The dendritic spikes are well separated from the larger somatic spikes. Similar results were obtained in nine other cells.

**DSGC Dendrites Are Excitable**

In order to directly test whether the dendrites of DSGCs are electrically excitable, we performed calcium imaging experiments. DSGCs were filled with the calcium indicator Oregon Green BAPTA-1 by passive diffusion from the patch electrode during current-clamp recordings. The DSGC was simultaneously stimulated with visible light along the preferred null axis while calcium signals were measured using 930 nm excitation from the infrared laser. As noted above, DSGCs comprise two planar dendritic arbors: an ON dendritic arbor (colored green in Figure 7A) and an OFF dendritic arbor (colored red in Figure 7A). Changes in the dendritic calcium concentration were measured as changes in fluo-

rescence intensity relative to the background. Calcium transients showed the same dependence on stimulus direction as the somatic spikes recorded in the same cell (Figure 7B), indicating that the fluorescence signal scaled linearly with the number of somatic spikes.

Leading and trailing edge responses produced calcium transients in both dendritic arbors (Figure 7C), indicating that a somatic spike resulting from stimulation of one dendritic arbor backpropagates and generates a calcium transient throughout the cell. Bath application of TTX, which blocks all spikes, reversibly abolished the calcium signals (Figure 7D), demonstrating that the depolarization produced by the PSPs was not sufficient to activate the dendritic calcium channels.

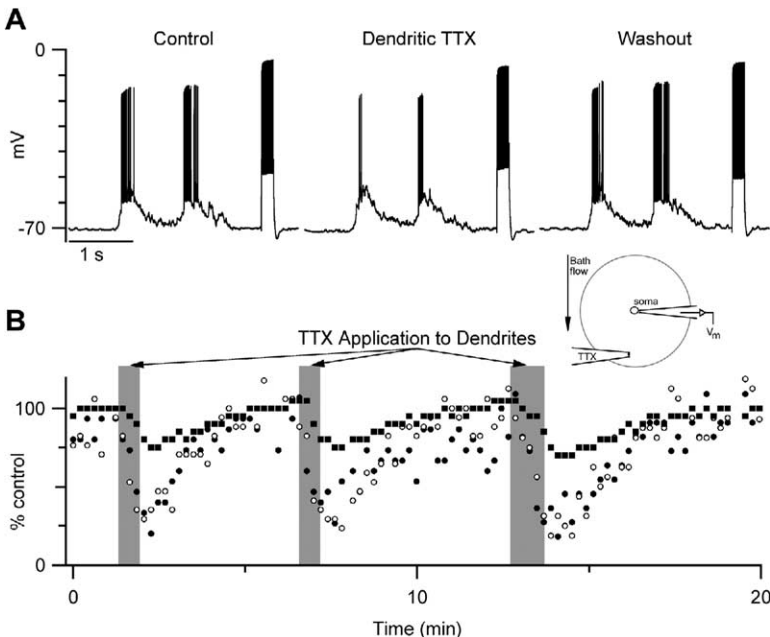


**Figure 6. TTX Application to the Dendrites Blocks Light-Evoked Spikes**

(A) Current-clamp responses to a dark bar moving in the preferred direction followed by a 500 pA current step 200 ms long. The inset schematic shows the positions of the TTX and recording electrodes in relation to the soma and dendrites (outer circle).

(B) Normalized spike counts expressed as percent spikes relative to pre-TTX application for ON spikes (open circles), OFF spikes (filled circles), and depolarization spikes (filled squares). Gray regions indicate periods of TTX application to the dendrites.

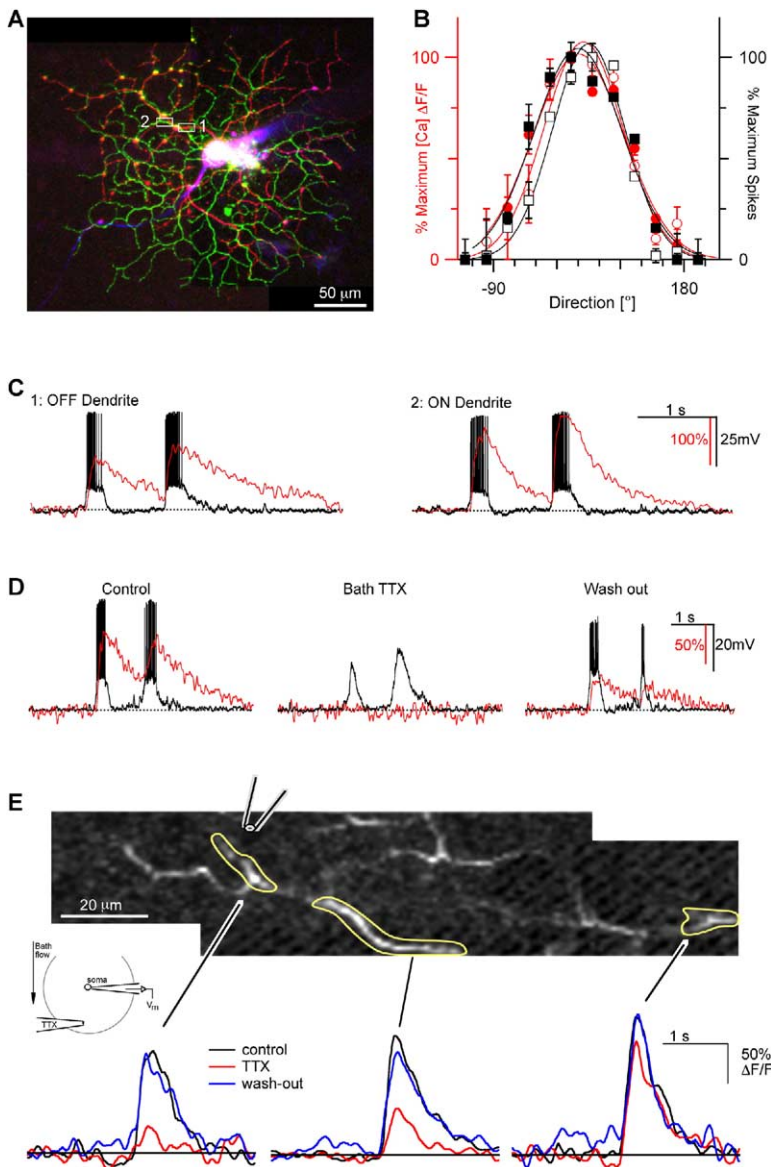


Figure 7. Dendrites Are Electrically Excitable Calcium imaging data are shown in red, and current-clamp data are shown in black. (A) Cell morphology showing the imaging locations in the OFF dendrites (C1) and ON dendrites (C2). In this pseudocolor image, the OFF dendrites are colored red, and the ON dendrites are colored green. The images of the two arbors have been overlaid for this illustration. During the experiments, only one dendritic arbor is visible, since the other lies well above or below the optical section. (B) The normalized magnitude of the calcium transients (left axis, red) and the number of action potentials (right axis, black) are plotted against the direction of stimulus motion. Each point represents the average response from three stimuli. The error bars show the standard error of the mean. (C) Responses were elicited by a preferred direction positive contrast stimulus. (C1) and (C2) show calcium transients and current-clamp responses in the OFF and ON dendritic arbor, respectively. (D) Voltage records and calcium signals in response to preferred direction stimuli, during control, 0.5  $\mu\text{M}$  bath TTX application, and washout. (E) TTX was applied to a section of dendrite as shown, and calcium transients were measured for each region of interest delineated by the white lines. Calcium transients were recorded during preferred direction stimuli before (black trace), during (red trace), and after (blue trace) TTX application.

Similarly, direct depolarization of the soma did not elicit calcium transients, until somatic spike threshold was reached, at which point calcium transients were again observed throughout the cell (data not shown).

The results indicate that the dendrites of DSGCs are electrically active. To directly test this, we applied TTX locally to a dendrite while presenting preferred direction light stimuli ( $n = 4$  cells; Figure 7E). The TTX suppressed calcium transients in dendrites close to the site of application, but not at more distant sites, providing direct evidence for the presence and physiological activation of TTX-sensitive sodium channels in the dendrites of the DSGCs.

## Discussion

We conclude from this study that spikes in DSGCs are initiated within the dendrites at more than one location, and that these dendritic spikes propagate toward the

soma, where they trigger somatic and axonal spikes. Dendritic spikes are not seen under control conditions because they are masked by the somatic spikes that they trigger. Generation of spikes locally within the dendrites enhances the directional tuning of the DSGCs.

## Evidence for Dendritic Spikes

Key evidence was obtained by the local application of TTX to the soma, which blocked large spikes and revealed the presence of dendritic spikes. An alternative explanation for the appearance of these small spikes is that TTX effectively reduces the sodium channel density at the soma and initial segment, with the result that action potentials do not reach the full amplitude. Under these conditions, one might expect to see a continuous variation of spike sizes due to the variable concentration of TTX present. However, examination of the spike amplitude distribution shows two discrete populations of spike amplitudes (Figure 3). The appearance of large

and small spikes within the same record suggests that local somatic TTX application can decrease the probability of somatic spike initiation before it has significant effects on the amplitude of the somatic action potentials.

Further evidence is the finding that hyperpolarization also suppresses large spikes and reveals small spikes. The same bimodal distribution in spike amplitudes is seen during this experimental condition as for the TTX application to the soma. This suggests that small spikes are not simply an artifact due to TTX reducing the number of active sodium channels but are always present and can be revealed if somatic spike initiation can be selectively suppressed. Moreover, hyperpolarization more readily unmasks dendritic spikes during ON responses. Such an observation provides strong evidence for the presence of at least two distinct spike initiation zones, one in each dendritic arbor.

Certain types of retinal ganglion cells that are coupled through gap junctions show evidence of electrical coupling, which can cause correlated firing (Bennett and Zukin, 2004; Brivanlou et al., 1998; Hidaka et al., 2004; Hu and Bloomfield, 2003; Mastrorarde, 1983). However, several lines of evidence indicate that the dendritic spikes that we recorded in DSGCs are not remnants of spikes activated in neighboring, electrically coupled neurons (MacVicar and Dudek, 1982; Valiante et al., 1995). First, there are four subtypes of DSGCs with distinct preferred directions corresponding to the four ocular cardinal directions. However, only one subset of DSGCs shows dye coupling (Vaney, 1994), whereas dendritic spikes are observed in all cells. Second, if DSGCs could transmit spikes to adjacent cells through gap junctions, then their receptive fields should be considerably larger than the dendritic extent; however, the receptive fields of the DSGCs are delineated by the extent of the dendritic arbors (Yang and Masland, 1994). Finally, the dendritic spikes have precisely the same preferred direction and directional tuning as the somatic spikes, which excludes the possibility that they originate in overlying DSGCs that have overlapping dendritic and receptive fields, but different preferred directions.

### Dendritic Spikes Trigger Somatic Spikes

By applying TTX locally to the dendrites of the DSGC, we were able to block a portion of the light-evoked spikes (Figure 6), which supports our hypothesis that dendritic action potentials propagate to the soma, where they initiate somatic spikes. Dendritic spikes are rarely seen under normal conditions, indicating that the probability that a dendritic spike will trigger a somatic spike is close to one. Our results also indicate that the spike threshold at the soma is set high, so that somatic spikes cannot be elicited by somatic PSPs, which are generated by the global summation of dendritic inputs and are similar in amplitude in the preferred and null directions (Figures 1 and 2). While spikes were clearly correlated with the occurrence of preferred direction PSPs, the apparent spike threshold was broadly distributed during the PSPs, suggesting that spike initiation was not strongly influenced by somatic membrane potential. This is consistent with the idea that incoming

dendritic spikes have a very high probability of initiating a somatic spike and that the depolarization represented by the somatic PSP does not significantly increase the probability of spiking.

### A Role for Dendritic Spikes

DSGCs receive directional excitatory and inhibitory synaptic inputs, with inhibition being larger in the null direction and excitation larger in the preferred direction (Borg-Graham, 2001; Fried et al., 2002; Taylor and Vaney, 2002). Directional inhibitory inputs are GABAergic and likely originate from starburst amacrine cells (Euler et al., 2002; Famiglietti, 2005; Fried et al., 2005). We show that the directional inputs produce PSPs that are weakly directional at the soma. We propose that the excitatory inputs will initiate dendritic spikes at local regions within the dendrites but that dendritic spikes generated during null direction motion will fail to propagate successfully to the soma due to directional inhibitory inputs from the starburst amacrine cells interposed between the spike initiation site and the soma. Precedence for this type of interaction has been shown in mitral cells (Chen et al., 1997; Kim et al., 1995; Lowe, 2002; Tsubokawa and Ross, 1996; Xiong and Chen, 2002) and pyramidal cells (Kim et al., 1995; Tsubokawa and Ross, 1996). The actual spike thresholds in the dendrites may be less important than judicious activation of postsynaptic inhibition, which should make the system more robust when the signal-to-noise ratio is unfavorable. Direct supporting evidence for this idea in DSGCs requires electrical recordings from the dendrites, a challenging prospect since the dendrites are typically 0.5  $\mu\text{m}$  in diameter (Amthor et al., 1984; He et al., 1999); however, other results support this interpretation of our findings.

DSGCs display a nondirectional zone that occurs on the preferred side of the receptive field (the side first encountered during preferred direction motion) and is evident by the appearance of spikes during null direction stimuli that traverse only the nondirectional zone (Barlow and Levick, 1965; He et al., 1999). Since inhibition is spatially offset toward the null direction (Barlow and Levick, 1965; Wyatt and Daw, 1975), inhibitory inputs will be interposed between the excitatory inputs and the soma on the null side of the dendritic arbor, but not on the preferred side (Figure 8). As a stimulus edge moves across the dendritic arbor in the null direction, the PSPs at local dendritic inputs near the edge will be mainly excitatory, and inputs onto dendrites ahead of the moving edge will be inhibitory (Figure 8, stimulus at N2). Dendritic spikes initiated by the excitatory inputs and propagating into the region of inhibition may fail due to the local shunting effect of the inhibitory conductance. However, if the null direction stimulus commences on the preferred side of the dendritic arbor (at P2), the inhibition will be activated distal to the excitation, and the dendritic spikes will propagate successfully to the soma. Thus, the existence and location of the nondirectional zone is consistent with the spatial arrangement of inhibition and excitation, and with our hypothesis that dendritic spike failure is more likely if the inhibition is on the path to the soma. These marked spatial differences in synaptic input are not reflected

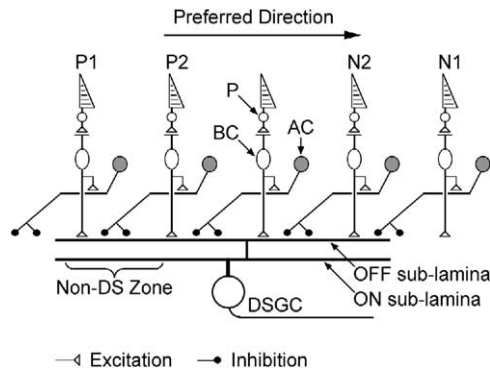


Figure 8. Synaptic Scheme

P, photoreceptor; BC, bipolar cell; AC, amacrine cell; DSGC, direction-selective ganglion cell. As the stimulus edge activates N2 during null direction motion, the inhibition activated ahead of the stimulus will cause spike failure. During preferred direction motion, the inhibition will be distal to the excitation over much of the receptive field, and dendritic spikes will successfully propagate to the soma. Within the non-DS zone, a stimulus moving in the null direction will first activate P2, and since inhibition is not activated between the excitatory inputs and the soma, dendritic spikes will generate somatic spikes. These spatiotemporal effects for motion in both directions will be complemented by presynaptic mechanisms, which generate directional inhibitory and excitatory inputs. Inhibition is larger in the null direction than the preferred direction, which will promote null direction dendritic spike failure. Excitation is smaller in the null direction than the preferred direction, which will tend to produce fewer null direction spikes. However, these motion-dependent presynaptic mechanisms cannot contribute to the offset in the spot-mapped receptive field toward the preferred side, as has been observed (see Discussion).

in current or voltage recordings from the soma, which comprise the summed input from all dendritic locations.

These same arguments can account for a systematic offset of the receptive field toward the preferred side of the dendritic field (Yang and Masland, 1994). While mapping the receptive field, a stimulus spot flashed on the null side of the dendritic arbor will activate on-the-path inhibition (Figure 8, stimulus at N2) and therefore will tend to produce fewer spikes than at the same relative location on the preferred side of the dendritic arbor (Figure 8, stimulus at P1). Thus, the receptive field will tend to be offset toward the preferred side, in agreement with observations (Yang and Masland, 1994).

Other results appear consistent with dendritic spike initiation. Excluding the nondirectional zone, directional spikes are generated by movements as small as  $\sim 40 \mu\text{m}$ , about 20% of the receptive field diameter (Barlow and Levick, 1965). A more recent study contends that the spatial resolution is 10-fold finer (Grzywacz et al., 1994). Thus, it seems that the critical directional mechanism is replicated many times across the receptive field. It is difficult to see how a single spike threshold at the soma could effectively discriminate preferred and null PSPs both for full field stimuli that produce large PSPs, and for restricted stimuli that produce smaller PSPs. A model that allows for local dendritic spike initiation can more easily explain these results.

The idea that directional selectivity may be the result

of local, postsynaptic, nonlinear interactions in the direction-selective (DS) cell was first introduced by Barlow and Levick (1965) and has received subsequent experimental (Amthor and Grzywacz, 1991, 1993; Taylor et al., 2000) and theoretical (Grzywacz et al., 1990; Grzywacz and Koch, 1987; Koch et al., 1982, 1983; Poggio and Reichardt, 1973; Torre and Poggio, 1978) support. The nonlinearity invoked in these studies was shunting inhibition, and it was generally agreed that such inhibition would need to be large, and in close proximity to excitatory inputs, to significantly shunt excitatory PSPs. Several studies have demonstrated that direction selectivity in DSGCs is dependent on GABA<sub>A</sub> receptors (Ariel and Daw, 1982; Caldwell et al., 1978; Kittila and Massey, 1997; Massey et al., 1997); however, anatomical analysis has shown that the patches of GABA receptors on DSGCs are not located immediately adjacent to the excitatory receptors (Jeon et al., 2002), and the present results show that depolarizing PSPs are seen during null direction motion. While our proposed model also invokes inhibitory shunting, since the inhibition promotes failure of dendritic spikes, it does not need to be close to the original excitation.

Recent work has emphasized the importance of presynaptic mechanisms for generating directional inputs to DSGCs (Borg-Graham, 2001; Euler et al., 2002; Fried et al., 2002; Taylor and Vaney, 2002). While directional signals are generated in the presynaptic circuitry, the current results show that local, postsynaptic processing within the dendrites of the DSGC is also important for producing sharply tuned directional signals.

## Experimental Procedures

### Tissue Preparation and Maintenance

Experiments were conducted in accordance with protocols approved by the Institutional Animal Care and Use Committee at OHSU and NIH guidelines. Dark-adapted, Dutch-belted rabbits were surgically anaesthetized, and their right eyes were removed under dim red illumination. The animals were then killed by anesthetic overdose. All subsequent manipulations were performed under infrared illumination ( $>900 \text{ nm}$ ) or under dim red light during the imaging experiments. The anterior portion of the eye was removed, the eyecup was transected just above the visual streak, and the dorsal piece was discarded. The retina was dissected from the sclera, and a  $5 \times 5 \text{ mm}$  section of central retina was adhered, photoreceptor side down, to a glass coverslip coated with poly-L-lysine (Sigma) or Cell-Tak (Becton Dickinson GmbH, Germany). The preparation was placed in a recording chamber ( $\sim 0.5 \text{ ml}$  volume) and continually perfused ( $\sim 4 \text{ ml/min}$ ) with oxygenated bicarbonate-buffered Ames medium (Ames and Nesbett, 1981), pH 7.4 maintained at  $34^\circ\text{--}36^\circ\text{C}$ . The major electrolytes in Ames medium are as follows: 120 mM NaCl, 23 mM NaHCO<sub>3</sub>, 3.1 mM KCl, 1.15 mM CaCl<sub>2</sub>, and 1.24 mM MgCl<sub>2</sub>.

### Electrophysiology and Light Stimulation

Patch electrodes were pulled from borosilicate glass to have a final resistance of 4–8 M $\Omega$ . For extracellular recording, the electrodes were filled with Ames medium. For intracellular recording, the electrodes were filled with the following electrolytes: 110 mM K-methylsulfonate, 10 mM NaCl, 5 mM Na-HEPES, 1 mM K-EGTA, 1 mM Na-ATP, and 0.1 mM Na-GTP. The liquid junction potential of 10 mV was subtracted from all voltages during analysis. Ganglion cells with a medium soma diameter and a crescent-shaped nucleus were targeted as potential DSGCs (Vaney, 1994). The extracellular electrode was applied to the soma under visual control through a small hole in the overlying inner limiting membrane, and a loose patch recording was formed. After establishing that the ganglion

cell was a DSGC and determining its preferred direction (see below), the extracellular recording electrode was removed, and an intracellular patch electrode was applied to the same cell. During whole-cell recordings, voltage signals were filtered at 2 kHz through the 4-pole Bessel filter of the Multiclamp 700A amplifier and digitized at 5–10 kHz. To minimize series resistance errors during whole-cell current-clamp recordings, 10 ms hyperpolarizing current pulses were applied and bridge-balanced to eliminate any instantaneous voltage offsets. Bridge balance was monitored periodically during the recordings.

TTX was applied locally to the soma or dendrites of the DSGCs from a patch electrode (4–8 M $\Omega$ ) positioned just above the cell. TTX at 0.2–1  $\mu$ M was dissolved directly into the extracellular Ames medium. The TTX was pressure ejected using a syringe. In some experiments, the lidocaine derivative QX-314 was included in the patch electrode. To ensure adequate time to obtain control responses, the tip of the electrode was filled with drug-free solution, and the electrode was backfilled with intracellular solution containing 1–10 mM QX-314. The drug diffused into the cell over a 10–20 min time period, during which we monitored the responses of the ganglion cells to depolarizing current pulses and preferred direction light stimuli.

Light stimuli, generated on a CRT computer monitor (refresh rate, 85 Hz), were focused onto the photoreceptor outer segments through a 20 $\times$  water-immersion objective (20 $\times$  0.95 W; XLUMPlanFI, Olympus). The percent stimulus contrast was defined as  $C = 100 \times (L - L_{mean})/L_{mean}$ , where  $L$  is the stimulus intensity and  $L_{mean}$  is the background intensity.  $C$  was set between 30% and 100%. The standard moving stimulus comprised a light or dark bar, moving along its long axis at 800–1200  $\mu$ m/s on the retina. All light stimuli were centered with respect to the tip of the recording electrode, and thus also with the soma of the ganglion cell. The bar's width was 250  $\mu$ m, and its length was set to achieve a 1–2 s separation of the leading edge and trailing edge responses. The stimulus area was limited by the aperture of the microscope objective and covered a circular region 1 mm in diameter. Since the dendritic extents of DSGCs, which delimit the receptive field (Yang and Masland, 1994), reach a maximum of about 400  $\mu$ m across in rabbit retina (Vaney, 1994), they were fully contained within the stimulus area. The leading edge of the stimulus bar commenced at one edge of the stimulus area and moved until the trailing edge reached the opposite edge. Thus, both leading and trailing edges of the stimulus traversed the whole receptive field of the recorded cell.

### Multiphoton Microscopy and Calcium Imaging

A custom-built upright multiphoton microscope equipped with a 20 $\times$  water-immersion lens (20 $\times$  0.95 W, XLUMPlanFI, Olympus) was used to identify and view cells, and to image calcium signals in dye-labeled cells (Denk and Detwiler, 1999; Euler et al., 2002). The tissue was counterstained with sulforhodamine 101 (2–4 mg/l; Sigma-Aldrich), which allowed us to visually identify the somata of DS ganglion cells with a high success rate. The sulforhodamine was usually washed out during recording periods to reduce fluorescence in the tissue and possible photodamage.

A mode-locked Ti:Sapphire laser (Mira-900; Coherent) tuned to 920–930 nm was used to excite the dyes. The scanning laser beam caused moderate and transient excitation of the DSGCs that adapted rapidly. Light stimuli overlaid upon the scanned region produced robust responses in the DSGCs. Thus, it was possible to visually stimulate DSGCs and optically record calcium signals simultaneously. Filters in the stimulation light path and in front of the detectors ("green" calcium signal: D 535 BP 50; "red" sulforhodamine counterstaining: HQ 622 BP 36) and dichroic mirrors in the optical path ensured that stimulus light did not interfere with fluorescence detection.

For calcium imaging, DSGCs were filled with Oregon Green BAPTA-1 (100–200  $\mu$ M in the pipette; Molecular Probes) via the patch pipette. The dye diffused rapidly into the dendritic tree so that imaging could commence within 3–5 min. The imaging software was developed at Bell Labs by R. Stepnoski and extended at the Max-Planck-Institute by M. Müller. Image regions (64  $\times$  8 pixel blocks at 62.5 Hz) or line scans (64 pixel lines at 500 Hz) were acquired from short dendritic segments and analyzed offline with

IgorPro (Wavemetrics). Fluorescence (F) data were spatially averaged over selected regions of interest and temporally filtered (line scans: box car, 10 ms window; image series: box car, 38 ms window). After background subtraction,  $\Delta F/F$  was calculated for each stimulus presentation. The maximal amplitude of the smoothed  $\Delta F/F$  trace was used to quantify the size of the calcium response.

Light stimuli were generated on a miniature LCD monitor (30 Hz frame rate; 800  $\times$  600 pixels with  $\sim$ 2.1  $\mu$ m/pixel; i-visor DH-4400VP, Cybermind Interactive, Netherlands), which was illuminated by a yellow LED, band-pass filtered (578 BP 10), and projected through the objective lens ( $\sim$ 1 mm field of view) onto the retina. An adjustable lens in the stimulus pathway offset the focal plane of the stimulus by about 100  $\mu$ m relative to the imaging plane. This ensured that the stimulus was focused on the photoreceptor array while the DSGC dendrites were imaged.

### Analysis

The preferred direction of the cells and the strength of the directional tuning were calculated from responses to stimuli in each of 12 stimulus directions evenly spanning 360°. Responses were represented as vectors, with the angle representing the direction of stimulus motion, and length equal to the number of action potentials or the peak amplitude of PSPs. The preferred direction was obtained from the angle of the resultant vector, obtained from the vector sum of all 12 responses. The DSI was calculated as the normalized length of the resultant vector. DSI can range from 0, when the magnitude of the response is the same in all stimulus directions, to 1, for perfect tuning when a response is produced only for a single stimulus direction (Taylor and Vaney, 2002). The directional tuning data in Figures 2 and 3 are well described by a von Mises distribution, which is the circular analog to the Gaussian distribution. The response  $R$ , as a function of stimulus direction is given as

$$R = R_{max} e^{(\kappa \cos((x - \mu) \pi / 180))} / e^{\kappa},$$

where  $R_{max}$  is the maximum response,  $\mu$  becomes the preferred direction in degrees, and  $\kappa$  is the concentration parameter, which accounts for the width of the directional tuning.

In some cells recorded PSPs were used as a current-clamp command waveform. The somatic input resistance was measured by applying hyperpolarizing current pulses. Then a preferred direction stimulus was applied, and the spikes on the resulting PSPs were digitally blanked. Digital spike blanking was performed by replacing the action potential with a straight line connecting a point preceding the threshold crossing to a point about 2 ms later. The resulting PSPs were then smoothed by digital filtering. Using the measured somatic input resistance, the PSPs were scaled to produce a series of current command waveforms that generated somatic PSPs, which bracketed the amplitude of the light-evoked PSPs.

Analysis was performed using custom procedures in IgorPro (Wavemetrics). Unless otherwise noted, the mean  $\pm$  standard deviation is quoted throughout the paper. Spikes were identified by threshold crossings of the second derivative of the current-clamp recordings. Differentiation effectively removed the slower PSPs and allowed the same detection threshold to be used regardless of fluctuations in the amplitude of the PSPs in the original voltage record. Spike times were detected as those events where the second derivative dropped below  $-2.10^5$  V/s<sup>2</sup>. A second threshold, usually set to 0 V/s<sup>2</sup>, signaled the end of the event. ISIs were determined from these spike times. The spike threshold potential was defined as the membrane potential at the time point, prior to the peak, where the second derivative exceeded  $-2.10^5$  V/s<sup>2</sup>. Essentially the same results were obtained using an alternative method in which spike threshold potentials were measured as the membrane potential at a fixed time (usually about 1 ms) before the peak. Spike amplitudes were calculated by subtracting the threshold potential from the membrane potential at the peak of the spike.

### Supplemental Data

The Supplemental Data include one figure and can be found with this article online at <http://www.neuron.org/cgi/content/full/47/5/739/DC1/>.

## Acknowledgments

Supported by NIH grant EY014888 to W.R.T., NHMRC (Australia) grant 179837 to D.I. Vaney and W.R.T., and the Max-Planck Society; the calcium imaging experiments were performed in W. Denk's laboratory. We wish to thank Drs. Winfried Denk, Rob Smith, and Salma Quraishi for helpful comments on the manuscript.

Received: January 11, 2005

Revised: May 31, 2005

Accepted: June 28, 2005

Published: August 31, 2005

## References

- Ames, A.I., and Nesbett, F.B. (1981). In vitro retina as an experimental model of the central nervous system. *J. Neurochem.* *37*, 867–877.
- Amthor, F., and Grzywacz, N. (1991). Nonlinearity of the inhibition underlying retinal directional selectivity. *Vis. Neurosci.* *6*, 197–206.
- Amthor, F.R., and Grzywacz, N.M. (1993). Inhibition in ON-OFF directionally selective ganglion cells of the rabbit retina. *J. Neurophysiol.* *69*, 2174–2187.
- Amthor, F.R., Oyster, C.W., and Takahashi, E.S. (1984). Morphology of on-off direction-selective ganglion cells in the rabbit retina. *Brain Res.* *298*, 187–190.
- Ariel, M., and Daw, N.W. (1982). Pharmacological analysis of directionally sensitive rabbit retinal ganglion cells. *J. Physiol.* *324*, 161–185.
- Barlow, H., and Levick, W. (1965). The mechanism of directionally selective units in rabbit's retina. *J. Physiol.* *178*, 477–504.
- Bennett, M.V., and Zukin, R.S. (2004). Electrical coupling and neuronal synchronization in the mammalian brain. *Neuron* *41*, 495–511.
- Borg-Graham, L. (2001). The computation of directional selectivity in the retina occurs presynaptic to the ganglion cell. *Nat. Neurosci.* *4*, 176–183.
- Brivanlou, I.H., Warland, D.K., and Meister, M. (1998). Mechanisms of concerted firing among retinal ganglion cells. *Neuron* *20*, 527–539.
- Caldwell, J., Daw, N., and Wyatt, H. (1978). Effects of picrotoxin and strychnine on rabbit retinal ganglion cells: lateral interactions for cells with more complex receptive fields. *J. Physiol.* *276*, 277–298.
- Chen, W.R., Midtgaard, J., and Shepherd, G.M. (1997). Forward and backward propagation of dendritic impulses and their synaptic control in mitral cells. *Science* *278*, 463–467.
- Denk, W., and Detwiler, P.B. (1999). Optical recording of light-evoked calcium signals in the functionally intact retina. *Proc. Natl. Acad. Sci. USA* *96*, 7035–7040.
- Djurisic, M., Antic, S., Chen, W.R., and Zecevic, D. (2004). Voltage imaging from dendrites of mitral cells: EPSP attenuation and spike trigger zones. *J. Neurosci.* *24*, 6703–6714.
- Euler, T., Detwiler, P.B., and Denk, W. (2002). Directionally selective calcium signals in dendrites of starburst amacrine cells. *Nature* *418*, 845–852.
- Famiglietti, E.V. (2005). Synaptic organization of complex ganglion cells in rabbit retina: Type and arrangement of inputs to directionally selective and local-edge-detector cells. *J. Comp. Neurol.* *484*, 357–391.
- Fohlmeister, J.F., and Miller, R.F. (1997). Mechanisms by which cell geometry controls repetitive impulse firing in retinal ganglion cells. *J. Neurophysiol.* *78*, 1948–1964.
- Fried, S.I., Munch, T.A., and Werblin, F.S. (2002). Mechanisms and circuitry underlying directional selectivity in the retina. *Nature* *420*, 411–414.
- Fried, S.I., Munch, T.A., and Werblin, F.S. (2005). Directional selectivity is formed at multiple levels by laterally offset inhibition in the rabbit retina. *Neuron* *46*, 117–127.
- Golding, N.L., and Spruston, N. (1998). Dendritic sodium spikes are variable triggers of axonal action potentials in hippocampal CA1 pyramidal neurons. *Neuron* *21*, 1189–1200.
- Grzywacz, N.M., and Koch, C. (1987). Functional properties of models for direction selectivity in the retina. *Synapse* *1*, 417–434.
- Grzywacz, N.M., Amthor, F.R., and Mistler, L.A. (1990). Applicability of quadratic and threshold models to motion discrimination in the rabbit retina. *Biol. Cybern.* *64*, 41–49.
- Grzywacz, N.M., Amthor, F.R., and Merwine, D.K. (1994). Directional hyperacuity in ganglion cells of the rabbit retina. *Vis. Neurosci.* *11*, 1019–1025.
- Hausser, M., Spruston, N., and Stuart, G.J. (2000). Diversity and dynamics of dendritic signaling. *Science* *290*, 739–744.
- He, S., Jin, Z.F., and Masland, R.H. (1999). The nondiscriminating zone of directionally selective retinal ganglion cells: comparison with dendritic structure and implications for mechanism. *J. Neurosci.* *19*, 8049–8056.
- Hidaka, S., Akahori, Y., and Kurosawa, Y. (2004). Dendrodendritic electrical synapses between mammalian retinal ganglion cells. *J. Neurosci.* *24*, 10553–10567.
- Hu, E.H., and Bloomfield, S.A. (2003). Gap junctional coupling underlies the short-latency spike synchrony of retinal  $\alpha$  ganglion cells. *J. Neurosci.* *23*, 6768–6777.
- Huguenard, J., Hamill, O., and Prince, D. (1998). Sodium channels in dendrites of rat cortical pyramidal neurons. *Proc. Natl. Acad. Sci. USA* *86*, 2473–2477.
- Jeon, C.J., Kong, J.H., Strettoi, E., Rockhill, R., Stasheff, S.F., and Masland, R.H. (2002). Pattern of synaptic excitation and inhibition upon direction-selective retinal ganglion cells. *J. Comp. Neurol.* *449*, 195–205.
- Kasuga, A., Enoki, R., Hashimoto, Y., Akiyama, H., Kawamura, Y., Inoue, M., Kudo, Y., and Miyakawa, H. (1993). Optical detection of dendritic spike initiation in hippocampal CA1 pyramidal neurons. *Neuroscience* *118*, 899–907.
- Kim, H.G., Beierlein, M., and Connors, B.W. (1995). Inhibitory control of excitable dendrites in neocortex. *J. Neurophysiol.* *74*, 1810–1814.
- Kittila, C., and Massey, S. (1997). Pharmacology of directionally selective ganglion cells in the rabbit retina. *J. Neurophysiol.* *77*, 675–689.
- Koch, C., Poggio, T., and Torre, V. (1982). Retinal ganglion cells: A functional interpretation of dendritic morphology. *Philos. Trans. R. Soc. Lond. B Biol. Sci.* *298*, 227–264.
- Koch, C., Poggio, T., and Torre, V. (1983). Nonlinear interactions in a dendritic tree: localization, timing, and role in information processing. *Proc. Natl. Acad. Sci. USA* *80*, 2799–2802.
- Larkum, M.E., Zhu, J.J., and Sakmann, B. (2001). Dendritic mechanisms underlying the coupling of the dendritic with the axonal action potential initiation zone of adult rat layer 5 pyramidal neurons. *J. Physiol.* *533*, 447–466.
- Llinas, R., and Nicholson, C. (1971). Electrophysiological properties of dendrites and somata in alligator Purkinje cells. *J. Neurophysiol.* *34*, 532–551.
- Lowe, G. (2002). Inhibition of backpropagating action potentials in mitral cell secondary dendrites. *J. Neurophysiol.* *88*, 64–85.
- MacVicar, B.A., and Dudek, F.E. (1982). Electrotonic coupling between granule cells of rat dentate gyrus: physiological and anatomical evidence. *J. Neurophysiol.* *47*, 579–592.
- Martina, M., Vida, I., and Jonas, P. (2000). Distal initiation and active propagation of action potentials in interneuron dendrites. *Science* *287*, 295–300.
- Massey, S.C., Linn, D.M., Kittila, C.A., and Mirza, W. (1997). Contributions of GABAA receptors and GABAC receptors to acetylcholine release and directional selectivity in the rabbit retina. *Vis. Neurosci.* *14*, 939–948.
- Mastroradar, D.N. (1983). Correlated firing of cat retinal ganglion cells. I. Spontaneously active inputs to X- and Y-cells. *J. Neurophysiol.* *49*, 303–324.
- Pinato, G., and Midtgaard, J. (2005). Dendritic sodium spikelets and

- low-threshold calcium spikes in turtle olfactory bulb granule cells. *J. Neurophysiol.* 93, 1285–1294.
- Poggio, T., and Reichardt, W. (1973). Considerations on models of movement detection. *Kybernetik* 13, 223–227.
- Regehr, W., Kehoe, J., Ascher, P., and Armstrong, C. (1993). Synaptically triggered action potentials in dendrites. *Neuron* 11, 145–151.
- Schwindt, P.C., and Crill, W.E. (1997). Local and propagated dendritic action potentials evoked by glutamate iontophoresis on rat neocortical pyramidal neurons. *J. Neurophysiol.* 77, 2466–2483.
- Spencer, W.A., and Kandel, E.R. (1961). Electrophysiology of hippocampal neurons. IV. Fast prepotentials. *J. Neurophysiol.* 24, 272–285.
- Spruston, N., Schiller, Y., Stuart, G., and Sakmann, B. (1995). Activity-dependent action potential invasion and calcium influx into hippocampal CA1 dendrites. *Science* 268, 297–300.
- Stuart, G.J., and Sakmann, B. (1994). Active propagation of somatic action potentials into neocortical pyramidal cell dendrites. *Nature* 367, 69–72.
- Stuart, G., Schiller, J., and Sakmann, B. (1997). Action potential initiation and propagation in rat neocortical pyramidal neurons. *J. Physiol.* 505, 617–632.
- Taylor, W.R., and Vaney, D.I. (2002). Diverse synaptic mechanisms generate direction selectivity in the rabbit retina. *J. Neurosci.* 22, 7712–7720.
- Taylor, W.R., and Vaney, D.I. (2003). New directions in retinal research. *Trends Neurosci.* 26, 379–385.
- Taylor, W.R., He, S., Levick, W.R., and Vaney, D.I. (2000). Dendritic computation of direction selectivity by retinal ganglion cells. *Science* 289, 2347–2350.
- Torre, V., and Poggio, T. (1978). A synaptic mechanism possibly underlying directional selectivity to motion. *Proc. R. Soc. Lond. B Biol. Sci.* 202, 409–416.
- Tsubokawa, H., and Ross, W.N. (1996). IPSPs modulate spike back-propagation and associated  $[Ca^{2+}]_i$  changes in the dendrites of hippocampal CA1 pyramidal neurons. *J. Neurophysiol.* 76, 2896–2906.
- Turner, R.W., Meyers, D.E., and Barker, J.L. (1989). Localization of tetrodotoxin-sensitive field potentials of CA1 pyramidal cells in the rat hippocampus. *J. Neurophysiol.* 62, 1375–1387.
- Turner, R.W., Meyers, D.E., Richardson, T.L., and Barker, J.L. (1991). The site for initiation of action potential discharge over the somatodendritic axis of rat hippocampal CA1 pyramidal neurons. *J. Neurosci.* 11, 2270–2280.
- Valiante, T.A., Perez Velazquez, J.L., Jahromi, S.S., and Carlen, P.L. (1995). Coupling potentials in CA1 neurons during calcium-free-induced field burst activity. *J. Neurosci.* 15, 6946–6956.
- Vaney, D.I. (1994). Territorial organization of direction-selective ganglion cells in rabbit retina. *J. Neurosci.* 14, 6301–6316.
- Vaney, D.I., and Taylor, W.R. (2002). Direction selectivity in the retina. *Curr. Opin. Neurobiol.* 12, 405–410.
- Velte, T.J., and Masland, R.H. (1999). Action potentials in the dendrites of retinal ganglion cells. *J. Neurophysiol.* 81, 1412–1417.
- Williams, S.R. (2004). Spatial compartmentalization and functional impact of conductance in pyramidal neurons. *Nat. Neurosci.* 7, 961–967. Published online August 22, 2004. 10.1038/nn1305.
- Wyatt, H.J., and Daw, N.D. (1975). Directionally sensitive ganglion cells in the rabbit retina: Specificity for stimulus direction, size and speed. *J. Neurophysiol.* 38, 613–626.
- Xiong, W., and Chen, W.R. (2002). Dynamic gating of spike propagation in the mitral cell lateral dendrites. *Neuron* 34, 115–126.
- Yang, G., and Masland, R.H. (1992). Direct visualization of the dendritic and receptive fields of directionally selective retinal ganglion cells. *Science* 258, 1949–1952.
- Yang, G., and Masland, R.H. (1994). Receptive fields and dendritic structure of directionally selective retinal ganglion cells. *J. Neurosci.* 14, 5267–5280.